Songklanakarin J. Sci. Technol.
39 (4), 451-461, Jul - Aug. 2017

http://www.sjst.psu.ac.th

Original Article

Experimental assessment on deformation and anisotropic behavior of saturated sandstone under cyclic loading

Wimon Sukplum* and Ladda Wannakao

Department of Geotechnology, Faculty of Technology,
Khon Kaen University, Mueang, Khon Kaen, 40002 Thailand

Received: 3 November 2015; Revised: 24 May 2016; Accepted: 8 July 2016

Abstract

The research was performed to assess the effects of cyclic loading on deformation behavior of saturated Phu Kradung sandstone of the Khorat Group under confining pressure and rock anisotropy. The cylindrical specimens were prepared for two orthogonal directions, normal and parallel (0 and 90 degree) to laminations to enable the anisotropic observation. Monotonic and cyclic loading tests were conducted under unconfined and confining pressures of 6, 12, 20 and 30 MPa. The results from both types of loading tests indicate that the level of confining pressure had a significant influence on the cyclic deformation of the saturated samples tested. The residual axial strains of samples obtained at a confining stress state can be described as three deformational stages, namely, the initial phase, uniform phase and final phase. The direction of loading in relation to its lamination demonstrates large difference in number of cycle reaching failure at unconfined stress condition, but insignificant effect under confined stress condition.

Keywords: monotonic loading, cyclic loading, saturated, confining pressure, Phu Kradung sandstone

1. Introduction

The mechanical behavior of rock mass under saturating and loading conditions are significance for the design and construction of roads, railways, highways, tunnel walls, rock fill dams, reservoirs, etc. The behavior of rock under static loading has been widely investigated. However, it is clear that the mechanical properties of rock under dynamic loads differ dramatically from those under static loads, the nature of dynamic failure in rock remains unclear, especially in cyclic loading condition (Xiao *et al.*, 2010). It is known that different materials show different responses under cyclic loading conditions. Some of these materials become stronger and more ductile, while others may become weaker and more brittle (Bagde & Petros, 2005a; 2005b). The mechanical behaviors of rock subjected to cyclic loading have been investigated extensively. Many researchers have carried out studies on different rock types to examine the loading effects and loading strain rates on their strength and deformation characteristics (Cho *et al.*, 2003; Liang *et al.*, 2011; Mahmutoglu, 2006; Ray *et al.*, 1999; Wang *et al.*, 2009; Zhao, 2000). Some researchers (e.g., Fuenkajorn & Phueakphum, 2010; Li *et al.*, 2001; Singh, 1989; Tien *et al.*, 1990) extensive work on cyclic loading was performed in order to determine whether rocks are subject to fatigue weakening. Furthermore, the correlation between the mechanical properties of dry and saturated rock samples have investigated (Li *et al.*, 2003; Kahraman, 2007; Winkler & McGowan, 2004). Anisotropy of construction materials can dictate their mechanical properties which are also crucial in design of engineering structures (Oliveira *et al.*, 2006). Rock masses are not exception their anisotropic behaviors can affect their mechanical properties tremendously (Amadei, 1996).

The studies cited above primarily focus on determining mechanical properties of dry rock samples condition, but a few studies have determined the mechanical

* Corresponding author.
Email address: wimosu@kku.ac.th

properties of saturated rock samples. Because, rock masses in the nature are both dry and saturated conditions. Therefore, this research investigated the mechanical behaviors on saturated specimens and their anisotropies under confining stresses as to provide more understanding on the saturated rock mechanical properties.

2. Rock Samples

The rock specimens in this investigation were taken from Phu Kradung Formation which is part of the Khorat Group that consists of continental red-beds which form most of the Khorat Plateau, Northeast Thailand. This Group is sub-divided into nine formations, namely from older to younger sequences as, Huai Hin Lat, Nam Phong, Phu Kradung, Phra Wihan, Sao Khua, Phu Phan, Khok Kruat, Mahasarakarm and Phu Thok Formations. The Khorat Group was dated as Upper Triassic to Cretaceous-Lower Tertiary as determined by fossil assemblage of vertebrates, bivalves and palyno-morphs (Stokes & Raksaskulwong, 2014). Rocks in the Khorat Group generally are sandstone, siltstone, and mudstone in each formation and exposed by folding structures as anticline and syncline on the Khorat plateau and its vicinity except in the southwestern part of the plateau, with overlying thick soil. The Phu Kradung Formation was generally formed through coarsening upwards succession in alluvial and fluvial floodplain of meandered river environment (Booth & Sattayarak, 2011) which its outcrops spread all over the borders of Khorat - Sakon Nakorn Basin. It has been involved in construction of several kinds such as the turbine tunnel of Lam Ta Khong Pumped Storage Project (Gurung & Iwao, 1998; Kaewkongkaew *et al.*, 2015). Mouret *et al.* (1993) divided the formation into two units. The lower unit consists of red-brown to grey-brown claystones and siltstones with thin bedded, fine-grained sandstone. The upper unit is typically thicker bedded, medium-grained sandstone (5-10 m. thick) and generally changes from reddish-brown to grey and white. The upper Phu Kradung sandstone is investigated in this research.

The sandstone specimens were core drilled from the in situ rock blocks at Nong Bualumpoo province, northeast Thailand, where this Phu Kradung sandstone Formation outcrop and transition contact to the younger Phra Wihan sandstones Formation. The core specimens of 54.50 mm in diameter were drilled in two orthogonal directions, normal and parallel (0 and 90 degree) to lamination (Figures 1 and 2). Specimens were cut, and lapped as specified by the ASTM D 4543-08 standard practice (American Society for Testing and Materials [ASTM] International, 2008). Twenty specimens were obtained for the basic properties and mechanical testing. All specimens were systematically labeled as to their rock formation (PK), orientation (S0 or S90), type of test (M, monotonic or C, cyclic), and their applied confining stress (0, 6, 12, 20, 30 MPa). The representative thin sections of the samples were also be prepared for petrographic examination.

2.1 Basic properties

Physical properties and mineral composition of the samples were determined in this study. Two physical properties i.e. density and porosity were evaluated for the specimens to be used for loading examinations. These properties were tested by water replacement method (ASTM International, 2015; International Society for Rock Mechanics [ISRM], 1981) and their values are shown along with the loading test results in Tables 1 and 2 the ranges of density and porosity values are 2.41 to 2.50 g/cm^3 and 5.75 to 9.83%, respectively.

The representative thin sections of the samples were also be prepared and used for petrographic examination. The mineral compositions of the rock samples were evaluated by two methods i.e. polarize microscope and X-ray diffraction.

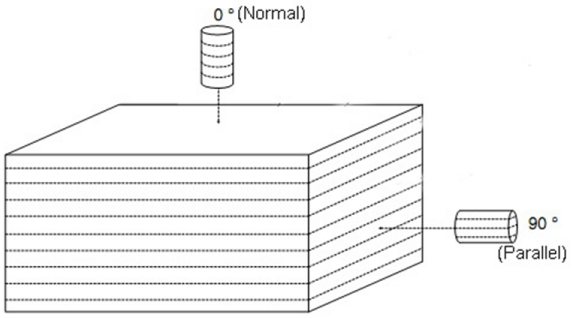

Figure 1. Coring orientation of the rock specimen.

Figure 2. Cylindrical specimens with two orthogonal directions.

Table 1. Basic properties of sample for monotonic loading test.

Sample no.	Wet density(g/cm^3)	Porosity(%)
PK-S0-0M	2.47	9.83
PK-S0-6M	2.49	5.75
PK-S0-12M	2.46	7.79
PK-S0-20M	2.46	8.90
PK-S0-30M	2.47	8.88
PK-S90-0M	2.49	7.82
PK-S90-6M	2.50	6.14
PK-S90-12M	2.50	5.89
PK-S90-20M	2.50	5.95
PK-S90-30M	2.46	6.73

Table 2. Basic properties of sample for cyclic loading test.

Sample no.	Wet density(g/cm^3)	Porosity(%)
PK-S0-0C	2.48	9.14
PK-S0-6C	2.46	9.20
PK-S0-12C	2.46	9.18
PK-S0-20C	2.47	8.98
PK-S0-30C	2.48	9.22
PK-S90-0C	2.46	6.86
PK-S90-6C	2.48	7.93
PK-S90-12C	2.50	8.15
PK-S90-20C	2.48	7.34
PK-S90-30C	2.41	8.46

The results are shown in Table 3 which indicates a high percentages of quartz, plagioclase feldspar and cemented with siliceous. Thus the rock was classified by used the Pettijohn classification of sandstone (Pettijohn, 1975) as arkosic sandstone.

3. Experimental Procedures

First of all, the core specimens were oven dried, and then soaked in the water for 24 hrs. After that, the experimental procedure was divided into two steps. First, the physical properties of specimens were determined, and then tested under monotonic and cyclic loading conditions. Saturated specimens were separated into two sets; the first set was monotonic tested to determine maximum strength of the rock at the confining stresses of 0, 6, 12, 20 and 30 MPa. Another set of core specimens were tested under cyclic loading at 70-80% of maximum stress level with the same confining stresses as the first set. The type and condition of loading tests are listed in Table 4. Detail testing procedures are as follows.

A 1,500 kN capacity, rock and concrete motorized compression test machine was used for both monotonic and cyclic loading tests. For monotonic testing, an unconfined compressive strength test follows the testing standard ASTM D7012-14(ASTM International, 2014). A Hoek cell was

Table 3. Mineral composition of the rock.

Optical microscope method Minerals (%)			X-ray diffraction method Minerals (%)		
Quartz	Plagioclase	Weathered feldspar	Quartz	Albite	Dickite
70	23-24	6-7	60.63	19.70	19.67

Table 4. Type and condition of loading tests.

Sample no.	Confining pressure (MPa)	Loading type	Loading condition
PK-S0-0M	0	Monotonic	Uniaxial, compression
PK-S0-0C	0	Cyclic	Uniaxial, 0.002 Hz, axial cyclic loading 0-35 kN
PK-S0-6M	6	Monotonic	Triaxial, compression
PK-S0-6C	6	Cyclic	Triaxial, 0.005 Hz, axial cyclic loading 14-100 kN
PK-S0-12M	12	Monotonic	Triaxial, compression
PK-S0-12C	12	Cyclic	Triaxial, 0.005 Hz, axial cyclic loading 28-136 kN
PK-S0-20M	20	Monotonic	Triaxial, compression
PK-S0-20C	20	Cyclic	Triaxial, 0.004 Hz, axial cyclic loading 44-216 kN
PK-S0-30M	30	Monotonic	Triaxial, compression
PK-S0-30C	30	Cyclic	Triaxial, 0.004 Hz, axial cyclic loading 68-280 kN
PK-S90-0M	0	Monotonic	Uniaxial, compression
PK-S90-0C	0	Cyclic	Uniaxial, 0.007 Hz, axial cyclic loading 0-32 kN
PK-S90-6M	6	Monotonic	Triaxial, compression
PK-S90-6C	6	Cyclic	Triaxial, 0.005 Hz, axial cyclic loading 14-152 kN
PK-S90-12M	12	Monotonic	Triaxial, compression
PK-S90-12C	12	Cyclic	Triaxial, 0.005 Hz, axial cyclic loading 28-200 kN
PK-S90-20M	20	Monotonic	Triaxial, compression
PK-S90-20C	20	Cyclic	Triaxial, 0.004 Hz, axial cyclic loading 44-260 kN
PK-S90-30M	30	Monotonic	Triaxial, compression
PK-S90-30C	30	Cyclic	Triaxial, 0.004 Hz, axial cyclic loading 68-320 kN

used for the triaxial compression test. A hydraulic jack with a maximum pressure of 70 MPa was used for applied confining pressure. Each specimen was placed in the Hoek cell and a confining stress applied and constantly controlled. The axial load was continuously applied until the specimen failed. The maximum axial stress (σ_1) of a certain confining stress was then determined; therefore, the applied cyclic stress could be estimated. Axial and lateral deformations were measured using electrical strain gauges for the uniaxial test. However, a mechanical gauge and oil volume change were used to record the axial and lateral deformations for the triaxial test.

All cyclic loading tests were carried out in the strain control mode. The test procedure follows the ASTM D7012-14 standard. The series of cyclic loading tests were performed at 70-80% of the predetermined uniaxial compressive strength (UCS) or confined compressive strength from monotonic tests; while, the minimum stress was maintained at hydrostatic stress level for triaxial test 6, 12, 20 and 30 MPa), A cyclic under uniaxial minimum applied load was at 0.4 kN - just enough to keep the platen in contact with the specimen. The axial and lateral strains were measured in each cycle until the specimen fails.

4. Results and Discussion

4.1 Monotonic loading tests

Uniaxial and triaxial compression tests were conducted to determine the rock's maximum strength at specified confining pressure; thus, the test parameters for subsequent cyclic loading tests could be predetermined. A summary of each specimen's confining stress and its strength are tabulated in Table 5 and, axial, lateral, and volumetric deformation behavior are illustrated in Figure 3. The stress-strain curves reveal that saturated sandstone samples exhibit brittle behavior for all the tests, especially under an unconfined compression test and at low confining pressure for the triaxial test. All of the specimens show axial contraction during loading and turn into dilation when loading is close to their strength.

4.2 Cyclic loading tests

The relationship between deviatory stress, volumetric strain, lateral strain and axial strain are plotted for uniaxial (Figure 4) and triaxial cyclic loading (Figures 5 and 6). The specimen's cyclic stress and number of cycles to failure are tabulated in Table 6. Results indicate that the number of cycles (*N*) increase with the increasing of the confining pressures. Loading in the direction of 0° to specimen lamination provides significantly higher N cycles than loading to the direction 90° at unconfined pressure. However, as confined pressures increases, the numbers of cycles are getting closer to each other; thus, indicating independency to the direction of loading (Figure 7). Deformation behaviors are observed when the axial cyclic load changes from the peak value (the maximal value in a cycle) to the valley value (the minimal value in a cycle). Axial deformation at the beginning of the loading cycle, the specimens exhibit elastic behavior; and, the deformation becomes more elastic – plastic as the loading cycle increases (Liu & He, 2012). As the confining pressure increases, larger axial strains are observed; especially when the failure cycle is reached. Axial, volumetric, and residual strains at failure are listed in Table 7. Other highlights noted are that the higher the confining pressure, specimens behave the more the ductility and the rock anisotropy also have influence on cyclic deformations. Axial strain and volumetric strain of the specimen's cyclic loading at 0° direction are larger than the 90° direction.

4.3 Effects of confining stresses on residual strain

Residual strain is defined as the strain (including axial, volumetric and lateral strains) at which the axial load reaches the valley value during the process of cyclic loading. When the axial cyclic load reduces to the minimal value in a cycle, some strain will be reversible and some remain irreversible this is the residual strain. Figure 8a-e present the relationship curves of the residual axial strain and the number of cycles (*N*) for 0° directional samples under unconfined and confined

Table 5. Basic properties and the stress state at failure.

Sample no.	Maximum strength (MPa)	Confining stress (MPa)
PK-S0-0M	10.52	0
PK-S0-6M	60.71	6
PK-S0-12M	74.04	12
PK-S0-20M	94.31	20
PK-S0-30M	128.69	30
PK-S90-0M	15.78	0
PK-S90-6M	83.49	6
PK-S90-12M	105.77	12
PK-S90-20M	119.39	20
PK-S90-30M	143.32	30

Table 6. Basic properties and number of cycles to failure.

Sample no.	Cyclic stress (MPa)	Cycles (N)
PK-S0-0C	15.78	11
PK-S0-6C	37.83	92
PK-S0-12C	47.60	124
PK-S0-20C	75.66	150
PK-S0-30C	93.43	185
PK-S90-0C	14.08	62
PK-S90-6C	55.44	86
PK-S90-12C	75.72	117
PK-S90-20C	95.02	142
PK-S90-30C	106.65	165

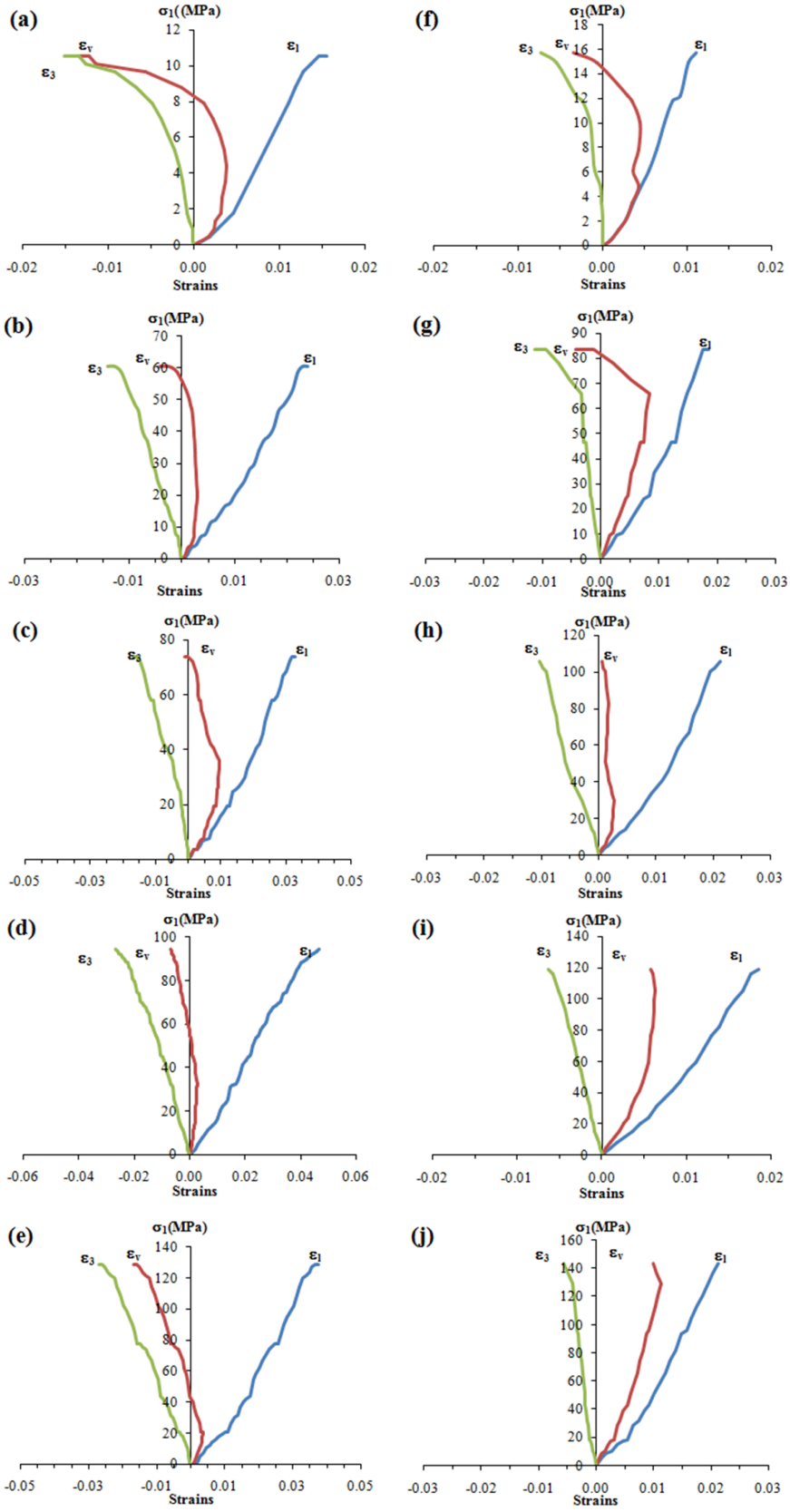

Figure 3. Stress-strain curves from uniaxial and triaxial compressive testing with monotonic loading of (a) PK-S0-0M, (b) PK-S0-6M, (c) PK-S0-12M, (d) PK-S0-20M, (e) PK-S0-30M, (f) PK-S90-0M, (g) PK-S90-6M, (h) PK-S90-12M, (i) PK-S90-20M and (j) PK-S90-30M.

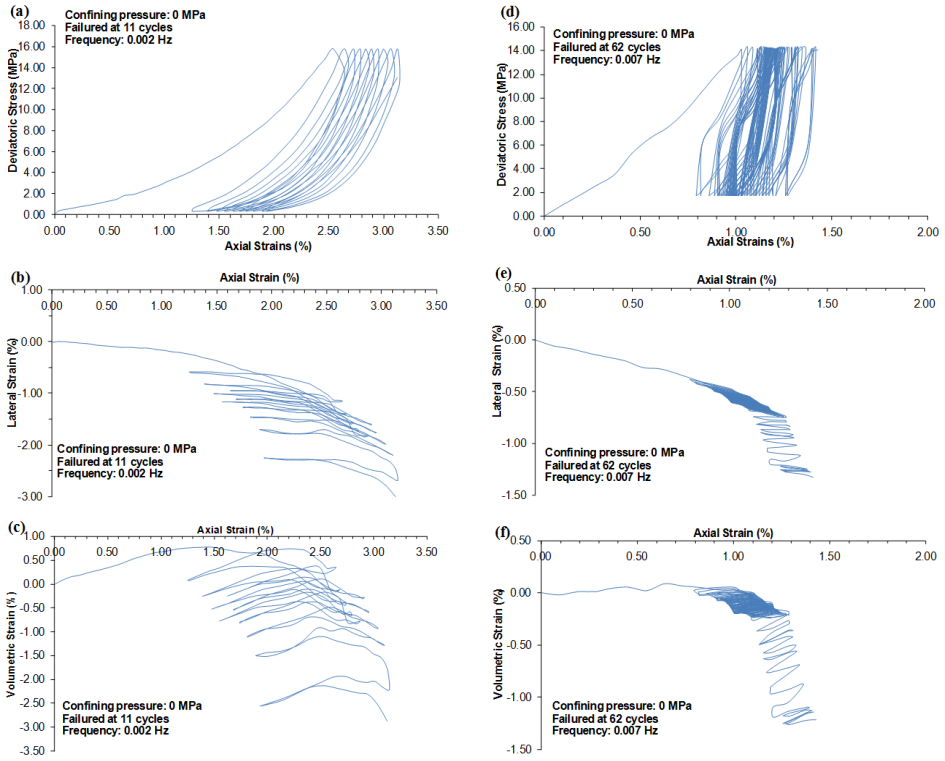

Figure 4. Uniaxial tests under cyclic loading (PK-S0-0C and PK-S90-0C) showing the relationships of axial strain to (a and d) deviatoric stress (b and e) lateral strain and (c and f) volumetric strain.

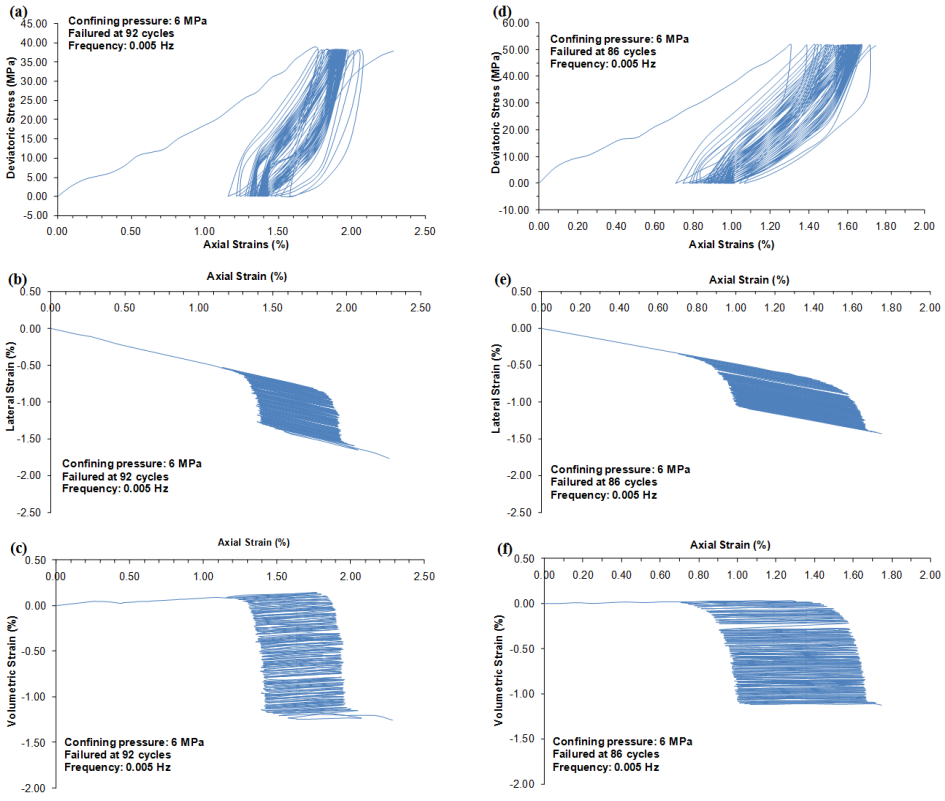

Figure 5. Triaxial tests under cyclic loading (PK-S0-6C and PK-S90-6C) showing the relationships of axial strain to (a and d) deviatoric stress (b and e) lateral strain and (c and f) volumetric strain.

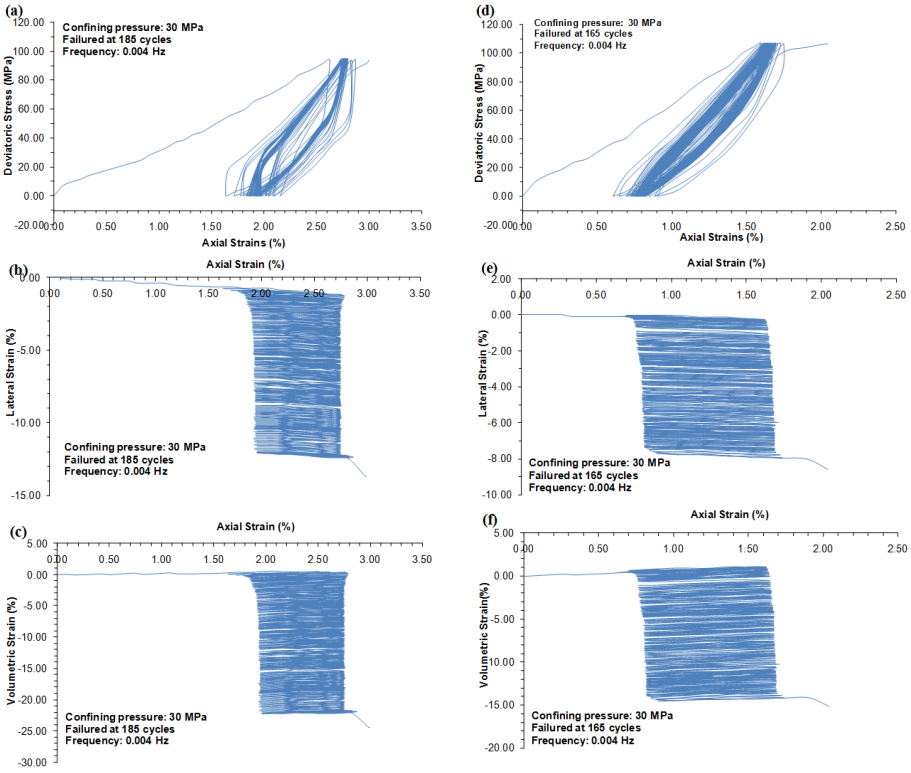

Figure 6. Triaxial tests under cyclic loading (PK-S0-30C and PK-S90-30C) showing the relationships of axial strain to (a and d) deviatoric stress (b and e) lateral strain and (c and f) volumetric strain.

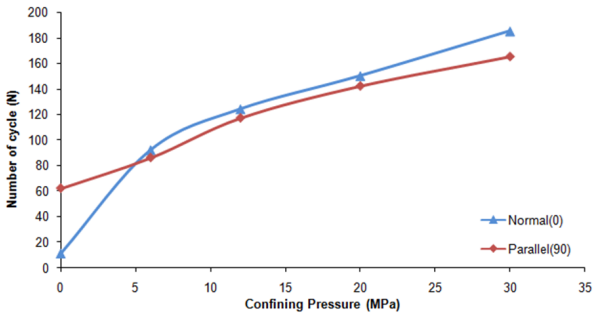

Figure 7. Relationships of confining pressure to number of cycle.

pressures at 6, 12, 20 and 30 MPa, respectively. Figure 8f-j also presents the relationship between the residual axial strain and the number of cycles (N) for 90° directional samples under unconfined and confined pressures at 6, 12, 20 and 30 MPa, respectively. Residual axial strain slowly increased at the beginning of loading cycles and then rapidly increased as the cycle got closer to the failure. Increasing of residual axial strain with number of loading cycles can be divided in three phases i.e. the initial phase, the uniform phase, and the final phase. The increments of residual axial strains are decreasing with number of cycles for initial phase. They are constant for the uniform velocity phase and increasing with acceleration

Table 7. Axial strain and volumetric strain at failure.

Sample no.	Axial strain (%)		Volumetric strain (%)	
	Maximum	Residual	Maximum	Residual
PK-S0-0C	3.125	1.930	-2.871	-2.559
PK-S0-6C	2.283	1.576	-1.253	-1.232
PK-S0-12C	2.749	2.100	-1.754	-1.625
PK-S0-20C	3.274	2.238	-2.281	-2.164
PK-S0-30C	3.658	2.735	-2.492	-2.274
PK-S90-0C	1.428	1.270	-1.217	-1.243
PK-S90-6C	1.748	1.065	-1.123	-1.118
PK-S90-12C	2.169	1.445	-1.590	-1.571
PK-S90-20C	2.514	1.717	-1.899	-1.804
PK-S90-30C	2.821	1.869	-2.064	-1.954

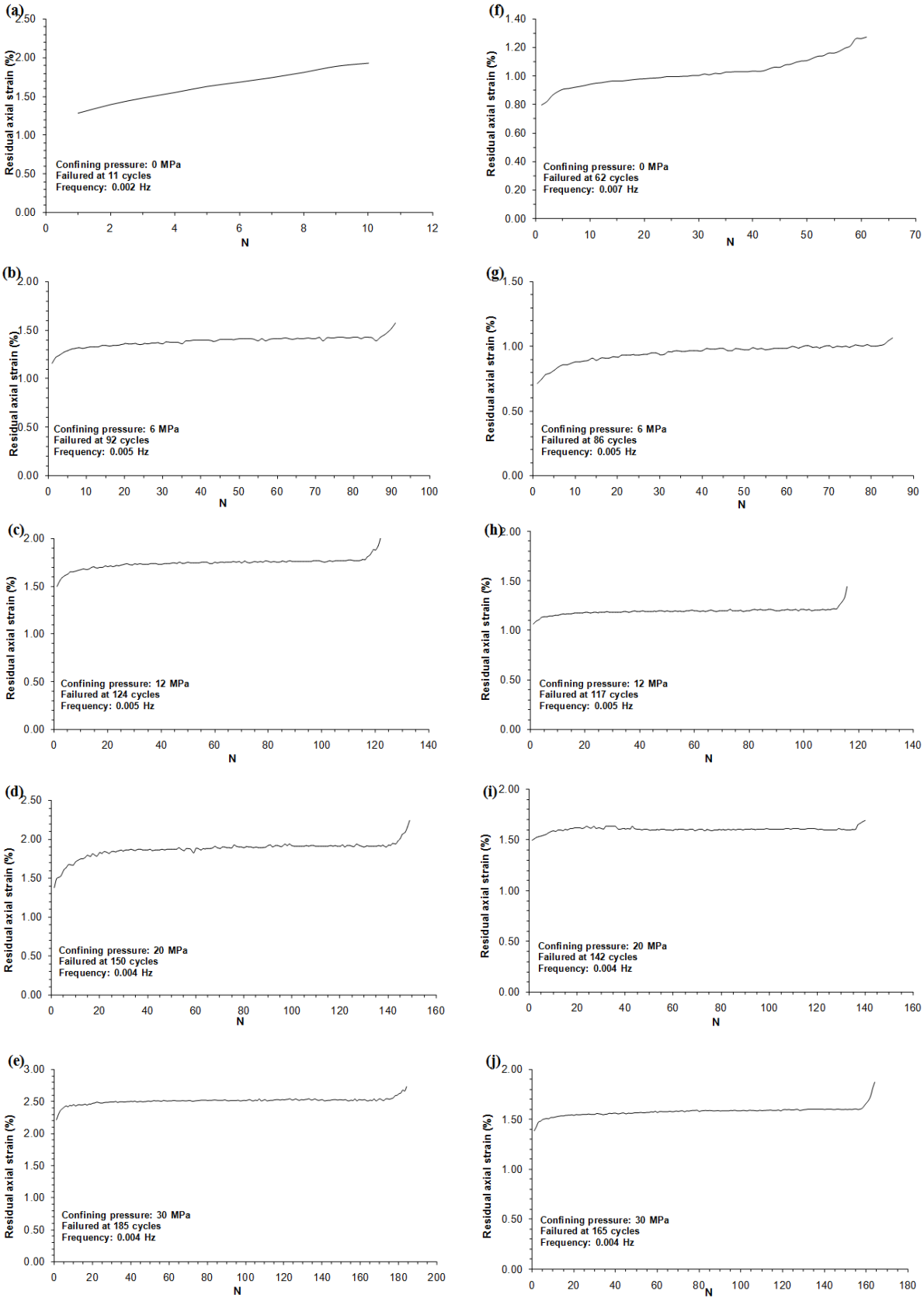

Figure 8. Residual axial strain-N curves (N: the number of cycles) for (a) PK-S0-0M, (b) PK-S0-6M, (c) PK-S0-12M, (d) PK-S0-20M, (e) PK-S0-30M, (f) PK-S90-0M, (g) PK-S90-6M, (h) PK-S90-12M, (i) PK-S90-20M and (j) PK-S90-30M.

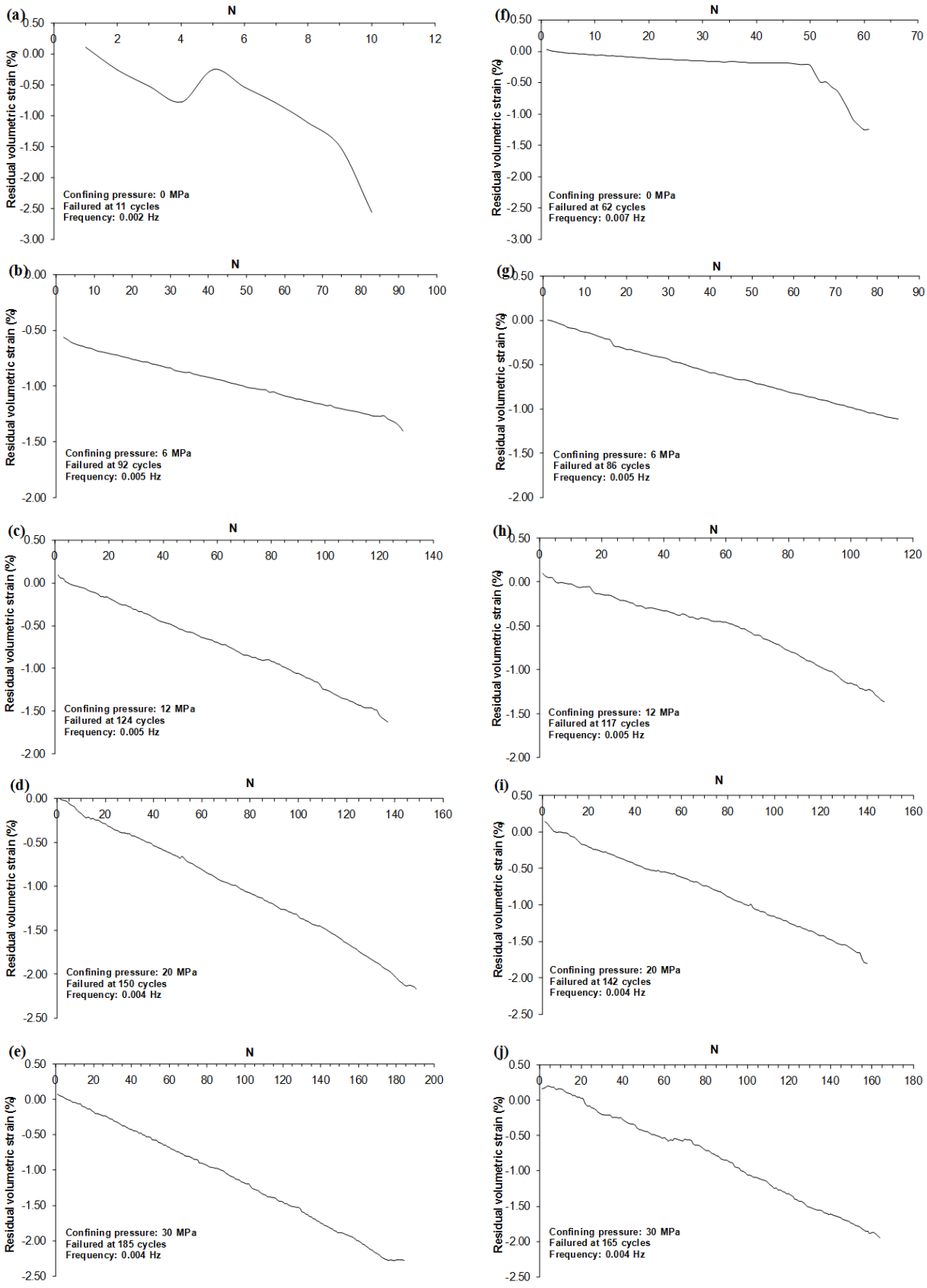

Figure 9. Residual volumetric strain-N curves (N: the number of cycles) for (a) PK-S0-0M, (b) PK-S0-6M, (c) PK-S0-12M, (d) PK-S0-20M, (e) PK-S0-30M, (f) PK-S90-0M, (g) PK-S90-6M, (h) PK-S90-12M, (i) PK-S90-20M and (j) PK-S90-30M.

manner for the final phase until failure. This phenomenal is compatible with the study of Liu and He (2012), Momeni *et al.* (2015), Sukplum and Wannakao (2016). Both the initial and final phases are short lives when compare to the uniform velocity phase (Figure 8). All the stages are completely found in the higher confining pressures. Figure 9a-e show the relationship between residual volumetric strain and the number of cycles (*N*) for 0° directional samples under unconfined and confined pressures at 6, 12, 20 and 30 MPa, respectively, Figure 9f-j illustrate the same relationship for the specimen orientation at 90° direction. Residual volumetric strains under uniaxial testing show influence of the lamination providing differing deformation behaviors. Significant additional contraction is demonstrated by specimens in the 0° direction. Under triaxial cyclic loading, small contraction occurs and then gradually expands as the volume changes. Similarly, the higher the confining pressures, the higher the volume changes.

5. Conclusions

This paper reports on a cyclic loading experiments investigation on the mechanical deformation properties of saturated sandstone under uniaxial and triaxial compression. Influence of the rock anisotropy is also investigated. The rock can be classified as arkosic sandstone according to mineral compositions. The following conclusions can be drawn: (1) the rock exhibits brittle deformation at lower cycles that turn into elastic-plastic deformation as indicated by larger axial and volumetric strains at higher cycles; (2) Three stages of deformation (initial, uniform and final phase) are established especially on triaxial cyclic loading; (3) Confining pressure has significant effect on deformation since the accelerated stage was easily detected with larger strains; and, (4) The orientation of lamination to direction of loading demonstrates a higher difference in the number of cycles to reach failure at uniaxial and low confining stresses. Additionally, the numbers of cycles are greater for loading parallel to lamination (specimens 90 ° direction). However, this effect shows very low or no influence on the number of cycles at greater confining stresses.

Acknowledgements

This research is funded by the Development and Promotion of Academic Fund for Academic Support and Graduate School, Khon Kaen University. Permission to publish this paper is gratefully acknowledged.

References

Amadei, B. (1996). Importance of anisotropy when estimating and measuring in situ stresses in rock. *International Journal of Rock Mechanics and Mining Sciences*, *33*(3), 293-325. doi: 10.1016/0148-9062(95)00062-3

American Society for Testing and Materials International. (2008). *ASTM D4543-08 standard practices for preparing rock core as cylindrical test specimens and verifying conformance to dimensional and shape tolerances*. Retrieved from https://www.astm.org

American Society for Testing and Materials International. (2014). *ASTM D7012-14 standard test methods for compressive strength and elastic moduli of intact rock core specimens under varying states of stress and temperatures*. Retrieved from https://www.astm.org

American Society for Testing and Materials International. (2015). *ASTM C127-15 Standard test method for relative density (specific gravity) and absorption of coarse aggregate.* Retrieved from https://www.astm.org

Bagde, M. N., & Petros, V. (2005a). Fatigue properties of intact sandstone samples subjected to dymamic uniaxial cyclical loading. *International Journal of Rock Mechanics and Mining Sciences*, *42*, 237-250. doi: 10.1016/j.ijrmms.2004.08.008

Bagde, M. N., & Petros, V. (2005b). The effect of machine behavior and mechanical properties of intact sandstone under static and dynamic uniaxial cyclic loading. *Rock Mechanics and Rock Engineering, 38*(1), 59-67. doi: 10.1007/s00603-004-0038-z

Booth, J., & Sattayarak, N. (2011). Subsurface carboniferous-Cretaceous geology of NE Thailand. In M. F. Ridd, A. J. Barber, & M. J. Crow (Eds.), *The geology of Thailand* (pp. 185-222). London, England: The Geological Society.

Cho, S. H., Ogata, Y., & Kaneko, K. (2003). Strain-rate dependentcy of the dynamic tensile stregth of rock. *International Journal of Rock Mechanics and Mining Sciences, 40*, 763-777. doi: 10.1016/S1365-1609(03)00072-8

Fuenkajorn, K., & Phueakphum, D. (2010). Effects of cyclic loading on mechanical properties of Maha Sarakham salt. *Engineering Geology, 112*, 43-52. doi: 10.1016/j.enggeo.2010.01.002

Gurung, N., & Iwao, Y. (1998). Observations of deformation and engineering geology in the Lam Ta Khong tunnel, Thailand. *Engineering Geology, 51*, 55-63. doi: 10.1016/S0013-7952(98)00031-3

International Society for Rock Mechanics. (1981). Rock characterization testing and monitoring ISRM suggested methods. In E. T. Brown (Ed.), *Suggested methods for determining water content, porosity, density, absorption and related properties* (pp.81-85). Oxford, England: Pergamon Press.

Kaewkongkaew, K., Phien-wej, N., & Kham-ai, D. (2015). Prediction of rock mass along tunnels by geostatistics. *KSCE Journal of Civil Engineering, 19*(1), 81-90. doi: 10.1007/s12205-014-0505-3

Kahraman, S. (2007). The correlations between the saturated and dry P-wave velocity of rocks. *Ultrasonics, 46,* 341-348. doi: 10.1016/j.ultras.2007.05.003

Li, N., Chen, W., Zhang, P., & Swoboda, G. (2001). The mechanical properties and fatigue-damage model for jointed rock masses subjected to dynamic cyclical loading. *International Journal of Rock Mechanics and Mining Sciences, 38*, 1071-1079. doi: 10.1016/S1365-1609(01)00058-2

Li, N., Zhang, P., Chen, Y., & Swoboda, G. (2003). Fatigue properties of cracked, saturated and frozen sandstone samples under cyclic loading. *International Journal of Rock Mechanics and Mining Sciences, 40*, 145-150. doi: 10.1016/S1365-1609(02)00111-9

Liang, W. G., Zhao, Y. S., Xu, S. G. & Dusseault, M. B. (2011). Effect of strain rate on the mechanical properties of salt rock. *International Journal of Rock Mechanics and Mining Sciences, 48*, 161-167. doi: 10.1016/j.ijrmms.2010.06.012

Liu, E. & He, S. (2012). Effect of cyclic dynamic loading on the mechanical properties of intact rock samples under confining pressure conditions. *Engineering Geology, 125*, 81-91. doi: 10.1016/j.enggeo.2011.11.007

Mahmutoglu, Y. (2006). The effect of strain rate and saturation on micro-cracked marble. *Engineering Geology, 82*, 137-144. doi:10.1016/j.enggeo.2005.09.001

Momeni, A., Karakus, M., Khanlari, G. R., & Heidari, M. (2015). Effecfs of cyclic loading on the mechanical properties of a granite. *International Journal of Rock Mechanics and Mining Sciences and Geomechanics, 77*, 89-96. doi: 10.1016/j.ijrmms.2015.03.029

Mouret, C., Heggemann, K., Gouadian, J., & Krisadasima, S. (1993). Geological history of the siliciclastic Mesozoic strata of the Khorat Group in the Phu Phan Range area, Northeastern Thailand. In T. Thanasuthipitak (Ed.), *Proceedings of the international symposium on biostratigraphy on mainland Southeast Asia: Facies and paleontology* (pp. 23-31). Chiang Mai, Thailand.

Oliveira, D. V., Lourenco, P. B., & Roca, P. (2006). Cyclic behavior of stone and brick masonry under uniaxial compressive loading. *Materials and Structures, 39* (2), 247-257. doi: 10.1617/s11527-005-9050-3

Ray, S. K., Sarkar, M., & Singh, T. N. (1999). Effect of cyclic loading and strain rate on the mechanical behaviour of sandstone. *International Journal of Rock Mechanics and Mining Sciences and Geomechanics, 36*, 543-549. doi: 10.1016/S0148-9062(99)00016-9

Pettijohn, F. J. (1975). *Sedimentary rocks*. New York, NY: Harper and Row.

Sigh, S. K. (1989). Fatigue and strain hardening behaviour of grawacke from the flagstaff formation, New South Wales. *Engineering Geology, 26*, 171-179. doi: 10.1016/0013-7952(89)90005-7

Stokes, B. R., & Raksaskulwong, M. (2014). Mesozoic Era, In T. Nuchanong *el al*. (Eds.), *Geology of Thailand: Department of Mineral Resources, Ministry of Natural Resources and Environment* (pp.113-155). Bangkok, Thailand.

Sukplum, W., & Wannakao, L. (2016). Influence of confining pressure on the mechanical behavior of Phu Kradung sandstone. *International Journal of Rock Mechanics and Mining Sciences, 86*, 48-54. doi: 10.1016/j.ijrmms.2016.04.001

Tien, Y. M., Lee, D. H., & Juang, C. H. (1990). Strain pore pressure and fatigue characteristics of sandstone under various load conditions. *International Journal of Rock Mechanics and Mining Science and Geomechanics Abstracts, 27*(4), 252-260. doi: 10.1016/0148-9062(90)90530-F

Wang, Q. Z., Li, W., & Xie, H. P. (2009). Dynamic split tensile test of flattened Brazilian disc of rock with SHPB setup. *Mechanics of Materials, 41*, 252-260. doi: 10.1016/j.mechmat.2008.10.004

Winkler, K. W., & McGowan, L. (2004). Nonlinear acousto-elastic constants of dry and saturated rocks. *Journal of Geophysical Research, 109*, B10204. doi: 10.1029/2004JB003262

Xiao, J. Q., Ding, D. X., Jiang, F. L., & Xu, G. (2010). Fatigue damage variable and evolution of rock subjected to cyclic loading. *International Journal of Rock Mechanics and Mining Sciences, 47*, 461-468. doi: 10.1016/j.ijrmms.2009.11.003

Zhao, J. (2000). Applicability of Mohr-Coulomb and Hoek-Brown strength criteria to the dynamic strength of brittle rock. *International Journal of Rock Mechanics and Mining Sciences, 37*, 1115-1121. doi: 10.1016/S1365-1609(00)00049-6